# Wide-area Transmission System Fault Analysis Based on Three-Phase State Estimation with Considering Measurement Errors


**Alireza Ghaedi and Mohammad Esmail Hamedani Golshan**

**Abstract** In this chapter, a wide-area integrated method including a set of algorithms for transmission lines fault analysis is introduced. The proposed method is based on extension and modification of state estimation formulation. Thus, the method is applicable to both symmetrical and asymmetrical networks as well as all fault types including symmetrical and asymmetrical ones. The method exploits the capacities of state estimation formulation and the solution algorithm of weighted least squares (WLS) to reduce the effect of inherent errors on the fault location accuracy and detection and elimination of bad data in the measurement vectors. For this purpose, an error model of the measurement chain including instrument transformers and PMUs is proposed. This model is used to design measuring errors covariance matrix in the state estimation formulation. The performance of the proposed method has been investigated through numerous fault events simulated on different locations of all transmission lines of the IEEE 118-bus test system.

**Keywords** Asymmetrical faults · Bad data detection · Fault location · Measurement chain error · State estimation · Untransposed transmission lines

## 1 Introduction

Expansion of transmission lines in vast geographical areas has caused these lines to be more exposed to natural phenomena such as lightning, windstorm, severe winds, floods, and human factors. These phenomena can lead to permanent faults

Springer-Verlag Tiergartenstr. 17, 69121 Heidelberg, Germany http://www.springer.com/lncs.

A. Ghaedi (✉) · M. E. Hamedani Golshan
Department of Electrical and Computer Engineering, Isfahan University of Technology, Isfahan 84156-83111, Iran
e-mail: a.ghaedi@ec.iut.ir

M. E. Hamedani Golshan
e-mail: hgolshan@cc.iut.ac.ir



H. Haes Alhelou et al. (eds.), *Wide Area Power Systems Stability, Protection, and Security*, Power Systems, https://doi.org/10.1007/978-3-030-54275-7_17

in transmission systems and long duration electricity interruption. That is why fault location studies have received much attention from the first days of transmission systems development. The higher accuracy of fault location speed up transmission line repair process. Consequently, network is restored to the normal state and power supply is reconnected for subscribers in the shortest possible time leading to higher system reliability.

A faulty line can usually be identified using protection systems or supervisory systems such as SCADA.[1] After that, finding the exact location of the fault is the main challenge lying ahead. The motivation behind this chapter is to present an integrated method which is able to estimate fault location, faulty line discrimination and fault type identification by using a number of wide-are phasor measurements. Another motivation is using a known and systematic framework for implementation of the integrated method and decreasing the effect of the inherent errors related to the measuring components on the method's results.

## *1.1 Literature Review and Background*

So that the preliminary research dates back to the 1930s. However, the importance of these methods became much more evident during World War II, and countries such as the United States, Canada, Belgium, France, and Japan obtained great achievements in this field [1]. An intensive plan was organized to develop fault location methods in Japan so that a team of professors from the University of Tokyo and representatives of nine power generating companies started collaborating as a "committee for fault location on transmission lines" [1]. Alongside these coherent activities in Japan, industrial companies each conducted separate research in the United States; however, according to a pre-arranged agreement between companies, there was a completely free exchange of information obtained from research. A comprehensive report by the AIEE[2] was published for the first time in order to review the existing methods and present future horizons of fault location studies [1]. Primary fault location methods can be classified into two main categories of visual inspection and fault location using fixed measurements [1]. Figure 1 summarizes this classification.

Primary methods of automatic fault location were unable to locate the fault. Some methods were only applicable to lines without power, so they could only detect permanent faults. However, to detect transient faults, the algorithms need either to be applied automatically to power lines or use the recorded data before the breakers can be opened. As such, fault location methods can be divided into two main groups:

– Traditional fault location methods
– Automatic fault location methods

[1] Supervisory Control and Data Acquisition.

[2] American Institute of Electrical Engineers.

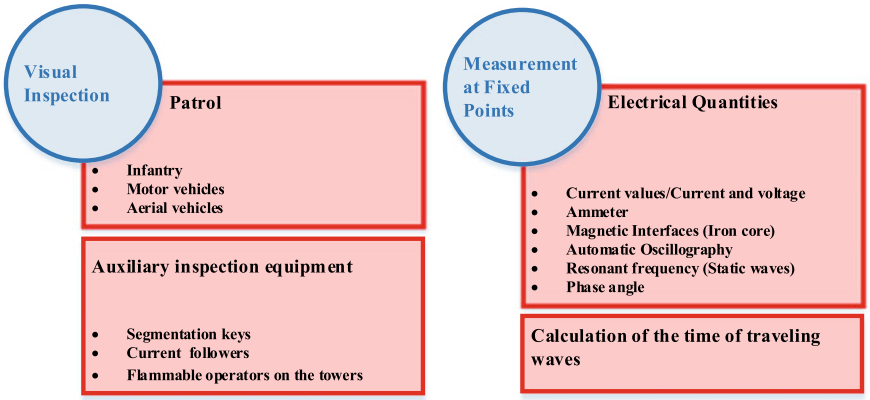


**Fig. 1** Primary fault location methods

### 1.1.1 Traditional Fault Location Methods

As mentioned earlier, traditional methods include a set of methods that cannot automatically detect the location of the fault in the aftermath of the fault, but patrols and maintenance teams should locate the fault by the use of equipment. Table 1 summarizes the traditional fault location methods used for overhead lines. Although many methods have been introduced so far, none of them were reliable methods for locating the fault. With the passage of time and the installation of equipment called "fault indicator" on the posts or transmission line towers, valuable information was provided to the users about the location of the fault. Then, the addition of radio features to fault indicators has made it possible to transmit fault-related information in impassable locations and bad weather conditions.

### 1.1.2 Automatic Fault Location Methods

Despite all the efforts made in different and unusual fault location methods, automatic fault location methods are still the most effective. These methods determine the physical location of the fault by processing the voltage and current waveforms. Most of the methods known today are among the automatic fault location methods. Automatic fault location methods can be categorized in terms of different aspects such as selection of appropriate frequency of under-study quantities, location of electrical quantities extraction, and choice of time/frequency domains. Meanwhile, in general, they can be divided into three main groups [2, 3], including traveling waves based methods, artificial intelligence-based methods, and main-frequency component-based methods. Each of the above-mentioned groups can be divided into two sub-sets of single-ended and two-ended in terms of used electrical quantities in the algorithm.

**Table 1** Summary of traditional fault location methods used for overhead lines [1]

| Row | Fault location method | Maximum algorithm error (%) | Implementation on power lines | Implementation on lines without power |
|---|---|---|---|---|
| 1 | Ammeter<br>The ammeters are faulty at the terminals leading to the line, so they roughly calculate the faulty area | 20% | Yes | No |
| 2 | Automatic oscillography<br>This is similar to the above method, with the exception that both voltage and current signals are used | 10% | Yes | No |
| 3 | Waves generated by the fault<br>The wave generated by a sudden voltage drop due to an occurred fault moves to the line terminals and is reflected continuously between the line post and the fault impedance. At the time of displacement, the wave is electrically measured and converted to circuit miles | 1% | Yes | No |
| 4 | Magnetic interfaces (Iron core)<br>It is similar to the automatic oscillographs method, except that the fault voltage and current are calculated by measuring the magnitude of the magnetic residues inside an iron core | 20% | Yes | No |
| 5 | Pulse radar<br>A pulse is applied to the line and the length of time the pulse is sent to and returns from the fault location is measured electrically. Then, the measured time is converted to circuit miles | 1% | Yes/No | Yes/Yes |
| 6 | Resonant frequency<br>A variable frequency source is connected to the line. At regular frequency intervals, the line itself exhibits a series resonance characteristic. The distance between these intervals is directly correlated with the distance of the source from the fault location | 2% | No | Yes |
| 7 | Flammable operators on the towers<br>The lightning current on the tower's legs creates visible light for patrol groups. This method uses currents caused by lightning or electrical faults to ignite some of the gunpowder embedded in the towers. Sparks created by the ignition of gunpowder remain in the air for some time, causing the tower connected to the fault location to be seen | 0% | Yes | No |
| 8 | Followers<br>A tracking signal is applied to the transmission line, which can be easily detected by portable devices. At the time of patrolling the line, a decrease in signal strength indicates a proximity to the fault point | 0% | Yes | No |

Decision making in traveling waves approaches is based on the analysis of the position-time graphs and the motion of the voltage and current waves [4, 5]. In this group of methods, several factors such as hard detection of initial traveling wave front and reflection wave front are considered as major challenges [4]. Numerous methods have been introduced to solve these challenges with defining new criteria [4, 6, 7]. In recent years, with the development of artificial intelligence-based methods in power system studies, these methods have also been used in fault location algorithms. These methods estimate fault location using tools such as support-vector machine (SVM) [8, 9] and extracting different characteristics of network signals [10]. The computational difficulties as well as the costs incurred to the power system in traveling wave-based methods and artificial intelligence-based ones have made impedance-based methods still very popular among researchers. Impedance method is considered as the most famous main-frequency component-based method. Impedance methods calculate the fault location directly through voltage and current phasors [11]. They calculate the fault location through the obtained data and without requiring any special hardware/software and as a result are highly economical [12]. However, they have disadvantages due to their dependence on faulty transmission line parameters and fault impedance [13]. Due to this dependence on various parameters, many studies have been conducted on the vulnerability of this group of algorithms [14]. Various types of impedance methods are investigated in [15] and different strategies are presented to improve their performance and reduce their errors. In contrast to two-ended methods, impedance-based methods that just use faulty single-ended data, do not require a communication link between the sending and receiving ends. On the other hand, less dependence on parameters in the two-ended methods results in an increase in the accuracy [15–18]. In addition to the introduced methods, a number of impedance-based methods have focused on determining fault location in the presence of high fault impedances. The main focus of these methods is on the phase to ground faults. As an instance, the method used in [19] uses the electrical quantities of both terminals and the faulty line parameters to estimate the fault location. Some methods such as [20, 21] estimate fault location by determining the Thevenin equivalent circuit of the network [20, 21]. Although these methods are the one-ended methods, they are able to greatly reduce the parameter dependency by taking advantage of equivalent circuit and statistical theories. Recently, impedance methods have been extended for multi-terminal transmission lines [22, 23] and nonhomogeneous transmission lines [24]. In the 80's, after introducing phasor measurement units (PMUs) [25], access to concurrent synchronous data was provided throughout the network. In addition to measuring the magnitude of voltages and currents, the equipment is also able to extract their phases. Additionally, the accuracy of PMUs measurements is far higher than that of other conventional measurement devices. The emergence of PMUs has led to the creation of another group of fault location algorithms called wide-are fault location methods (WAFL). This group of methods is able to estimate the fault location by measuring some of the network voltages and currents from different points, not necessarily the bus connected to the faulty line [26–30]. The wide area methods gained their popularity mainly due to their capability to decide on the location of the

occurred fault based on scattered information from the voltage and current phasors in the network [31, 32]. Some WAFL approaches have been introduced such as hybrid (synchronized and unsynchronized) measurements and non-iterative methods [33–35].

## *1.2 Contributions*

This study was carried out to overcome some common challenges of the fault location methods proposed over the last few decades. The error in estimating the fault location introduced by bad data and inherent errors in the measurement chains are some of these challenges. For this purpose, a novel algorithm based on the well-known formulation of system state estimation is proposed for fault location. The other challenge in fault location algorithms is how to encounter network asymmetries and asymmetric faults. In order to determine the fault location in the cases where the network is asymmetric, e.g. due to lack of fully transmission system transposition, and occurrence of asymmetric faults (single-line-to-ground, line-to-line, and double line-to-ground), the proposed algorithm is based on three-phase state estimation formulation. The proposed method is also able to determine the fault occurrence, fault type, and phases that contribute to fault, along with fault location. Therefore, the proposed method includes a set of algorithms based on the three-phase state estimation.

To tackle the mentioned challenges and goals, the basic three-phase state estimation algorithm is modified by considering the fault location as a hypothetical bus on which is not feasible to install a PMU. The voltage phasor of this hypothetical bus, the injected current (fault current) and the fault location are also added to the problem variables. Thus, the achievements presented in this innovative study are summarized as follows:

Proposing a set of algorithms based on the modified three-phase state estimation for fault detection, faulty line discrimination, fault location estimation and fault type and faulty phase(s) identification.
Exploiting the capacities of three-phase state estimation for locating all kinds of symmetrical and asymmetrical faults on transposed and untransposed lines.
Presenting an error model of the measurement chain including instrument transformers and PMUs.
Reducing the effect of inherent error measurement chain on the fault location accuracy and detecting and eliminating bad data in the measurement vectors based on the design of measuring errors covariance matrix in the state estimation formulation.

## 2 Three-Phase State Estimation

The most common faults in power systems are asymmetrical faults [36] and also transmission systems are mainly asymmetric due to lack of fully lines transposition. Thus, the formulation of three-phase state estimation has been expanded in this study for the possibility of considering asymmetric faults, incomplete lines transposition and network asymmetries.

The purpose of power system state estimation is to calculate the magnitude and phase angle of the voltage of all network buses (state variables) using the quantities measured at different points in the network. The general form of three-phase state estimation equations are as follows:

$$\overline{z} = \begin{bmatrix} \overline{z}_1 \\ \overline{z}_2 \\ . \\ . \\ . \\ \overline{z}_m \end{bmatrix} = \begin{bmatrix} \overline{h}_1(x_1, x_2, ..., x_n) \\ \overline{h}_2(x_1, x_2, ..., x_n) \\ . \\ . \\ . \\ \overline{h}_m(x_1, x_2, ..., x_n) \end{bmatrix} + \begin{bmatrix} \overline{e}_1 \\ \overline{e}_2 \\ . \\ . \\ . \\ \overline{e}_m \end{bmatrix} = \overline{h}(\overline{x}) + \overline{e} \tag{1}$$

In (1), $m$ shows the number of three-phase PMU measurement blocks. Thus, the vector of system measurements $\overline{z}$ includes magnitude and phase angle of buses voltages and lines currents and has the order of $3m \times 1$. The vector of measurement functions, $\overline{h}(\overline{x})$, includes relationships between measurements and state variables. The order of $\overline{h}(\overline{x})$ is $3m$. Assuming there are $N_{bus}$ buses in the network, the number of the state variables $n$ is equal to $6N_{bus}$ including three magnitudes and three-phase angles for voltage phasor of each bus. The vector of state variables is denoted by $\overline{x} = \left[x_1\ x_2\ ...\ x_n\right]^T$. The measurement errors vector is of the order of $3m \times 1$ and is denoted by $\overline{e}$.

One of the most commonly used methods for solving state estimation problem is weighted least squares (WLS) method [37]. The purpose of WLS estimator is to minimize the value of objective function of (2):

$$J(\overline{x}) = \left[\overline{z} - \overline{h}(\overline{x})\right]^T . R^{-1} . \left[\overline{z} - \overline{h}(\overline{x})\right] \tag{2}$$

where, matrix R is the measurement errors covariance matrix.

$$R = Cov(e) = E\left[\overline{e}.\overline{e}^T\right] = diag(\overline{\sigma_1^2},\ \overline{\sigma_2^2},\ ...,\ \overline{\sigma_m^2}) \tag{3}$$

Diagonal matrices $\overline{\sigma^2}_i$s indicate the variance of the measurements related to the $i$-th three-phase measurement block.

$$\overline{\sigma^2}_i = \begin{bmatrix} \sigma_{i_a}^2 & 0 & 0 \\ 0 & \sigma_{i_b}^2 & 0 \\ 0 & 0 & \sigma_{i_c}^2 \end{bmatrix}. \tag{4}$$

The necessary condition for optimal solution of $J(x)$ is as (5):

$$g(\overline{x}) = \frac{\partial J(\overline{x})}{\partial \overline{x}} = 0 \tag{5}$$

or

$$-H^T.R^{-1}.\left[\overline{z} - \overline{h}(\overline{x})\right] = 0 \tag{6}$$

where $H(\overline{x}) = \frac{\partial \overline{h}(\overline{x})}{\partial \overline{x}}$ is the Jacobian matrix of measurement functions. Using Taylor expansion and considering the linear approximation of $\overline{h}(\overline{x}^k + \Delta\overline{x}^k) \cong \overline{h}(\overline{x}^k) + H(\overline{x}^k).\Delta\overline{x}^k$, (6) can be written as:

$$H^T(\overline{x}^k).R^{-1}.H(\overline{x}^k).\Delta\overline{x}^k = H^T(\overline{x}^k).R^{-1}.\left[\overline{z} - \overline{h}(\overline{x}^k)\right] \tag{7}$$

where $\Delta\overline{x}^k = \overline{x}^{k+1} - \overline{x}^k$ and $\overline{x}^{k+1}$ and $\overline{x}^k$ denote the solutions of $(k+1)$-th and $k$-th steps of (7). By defining the gain or information matrix as

$$G(\overline{x}) = H^T.R^{-1}.H \tag{8}$$

and rearranging (7), the unknown $\overline{x}$ is obtained by the iterative solution of (9):

$$\overline{x}^{k+1} = \overline{x}^k - G(\overline{x}^k)^{-1}.g(\overline{x}^k) \tag{9}$$

The iteration process is continued until $\left|\Delta\overline{x}^k\right| < \varepsilon$ where $\varepsilon$ and $k$ are the convergence threshold of the problem solution and the iteration number in problem solution process, respectively.

## 3 The Proposed Method to Determine Matrix R

Determining the power system status requires measuring a number of network electrical quantities. Figure 3 shows how to extract the electrical quantities. The process shown in Fig, 3 is called "measurement process" or "measurement chain". Each measurement chain consists of two main components, namely an instrument transformer and a measuring device. Therefore, the measurement accuracy is directly affected by the accuracy of both instrument transformers and measuring devices. Equipment errors include the errors related to their inherent limitations and systematic or biased errors due to their failure or other reasons.

The inherent errors of the equipment in the measurement chain are declared by the equipment manufacturer. These errors should be in accordance with the national or international standards. The measurement error exists on both magnitude and phase angle of voltage and current signals (Fig. 2).

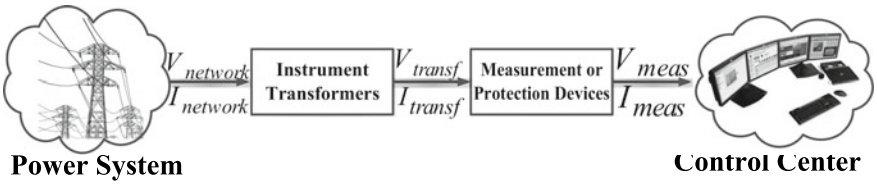


**Fig. 2** A typical measurement chain in power system

**Table 2** Maximum error of measurement devices [40]

| Conventional measurements | | PMU measurements | | |
|---|---|---|---|---|
| Active power | Reactive power | Voltage | Current | Phase angle |
| ±3% | ±3% | ±0.02% | ±0.03% | ±0.54° |

IEEE C57.13 standard has provided accuracy classes for instrument transformers [38]. Accordingly, the maximum error of voltage and current transformers depends on the power system operating condition.

For fault location, it is necessary to examine the network quantities during the fault. The protective instrument transformers are used to obtain the abnormal voltage and current during the fault. The maximum permissible error and the accuracy class for this equipment are given in [39]. Table 2 also shows the maximum possible error of measurement equipment in accordance with IEEE C37.118.1 standard [40]. To identify the accuracy of measurement chain, it is necessary to consider the maximum possible error occurring in both the intermediary transformers and measuring devices to determine the error of measurement chains. In the following, we examine the error of each measurement chain in terms of errors of its components.

For this purpose, popular statistical distributions for equipment error are used. Due to the features such as continuity, symmetric feature, and ultimately zero mean in standard mode, standard normal distribution has been used for modeling the errors. In other references, the standard normal distribution is also called error distribution [36]. Many engineering applications also use standard normal distribution to model the errors.

In the measurement chain shown in Fig. 3, the relationship between converted quantities ($F_{transf}$) and actual quantities of the network ($F_{network}$) is given by (10). The final value of quantities in the output of the measurement process used in the algorithms is also expressed as (11):

$$F_{transf} = F_{network} + N(0, u_{IT}^{F}) \tag{10}$$

$$F_{meas} = F_{transf} + N(0, u_{PMU}^{F}) \tag{11}$$

where $N(0, \sigma^2)$ expresses a normal distribution with the mean 0 and the variance $\sigma^2$. In (10) and (11), $u_{IT}^{F}$, and $u_{PMU}^{F}$ represent the standard uncertainty in the output

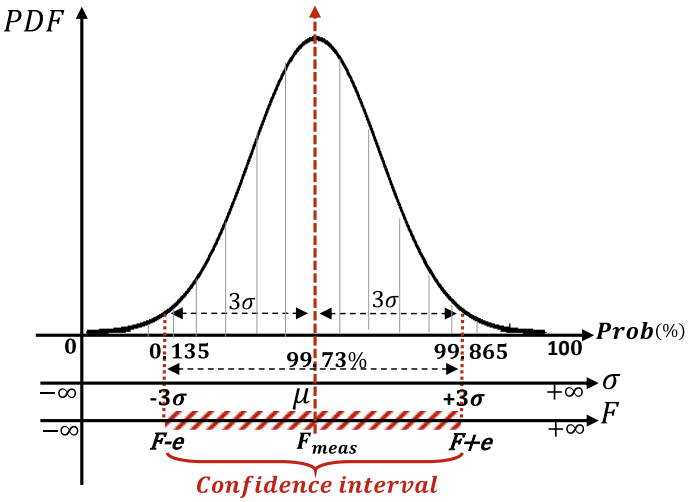


**Fig. 3** Standard normal distribution and parameters definition

quantities of voltage/current transformers and PMUs, respectively. Furthermore, $F$ is used to represent the measured quantities including $V$ (voltage magnitude), $I$ (current magnitude), $\theta^V$ (voltage phase angle), and $\theta^I$ (current phase angle). $IT$ is also used to represent voltage transformer (VT) or current transformer (CT). Therefore, it is expected that the converted quantities and measured values lie within the confidence intervals:

$$(1 - e_{IT})F_{network} < F_{transf} < (1 + e_{IT})F_{network} \tag{12}$$

$$F_{transf}(1 - e_{PMU}) < F_{meas} < F_{transf}(1 + e_{PMU}) \tag{13}$$

where $e^F_{IT}$ and $e^F_{PMU}$ are the maximum possible error of magnitude or phase angle for the instrument transformers and PMUs, respectively. It should be noted that due to the stochastic nature of the measuring process, the obtained quantities may not be contained in the confidence interval. The probability of the obtained quantities being within the confidence interval is defined as level of confidence ($p$). For example, consider a voltage magnitude measurement, it is expected that the obtained value reflects the confidence interval $0.98\left|V_{transf}\right| < |V_{meas}| < 1.02\left|V_{transf}\right|$ that is 99.73%. In the other words:

$$Prob(0.98\left|V_{transf}\right| < |V_{meas}| < 1.02\left|V_{transf}\right|) = 99.73\% \tag{14}$$

It means that from each 1,000 measured samples, 3 samples are out of the confidence interval. Since in a power system, samples are continuously extracted, their behavior can be described by the standard normal distribution. The confidence interval, confidence level and its relation are shown in Fig. 3.

**Table 3** Value of the coverage factor $k_p$ that produces an interval having level of confidence $p$ assuming a standard normal distribution

| Level of confidence $p$ (%) | Coverage factor $k_p$ |
|---|---|
| 90 | 1.645 |
| 95 | 1.96 |
| 95.45 | 2 |
| 99 | 2.576 |
| 99.73 | 3 |

Uncertainties of voltage and current magnitudes in the standard normal distribution are obtained by the following equations [36]:

$$u_{IT}^{F}.k_p = e_{IT}^{F}\,|F_{meas}| \tag{15}$$

$$u_{PMU}^{F}.k_p = e_{PMU}^{F}\,|F_{meas}| \tag{16}$$

where $k_p$ represents coverage factor and $|F_{meas}|$ is the magnitude of voltage or current sent to the control center. The different $k_p$s corresponding to various values of $p$ are presented in Table 3. If $F$ means the voltage or current phase angle, uncertainties in the standard normal distribution are presented as follows:

$$u_{IT}^{F}.k_p = e_{IT}^{F} \tag{17}$$

$$u_{PMU}^{F}.k_p = e_{PMU}^{F} \tag{18}$$

By substituting (10) in (11), equation (19) is obtained.

$$F_{meas} = F_{network} + N(0, u_{IT}^{F}) + N(0, u_{PMU}^{F}) \tag{19}$$

As instrument transformers and PMUs are separate equipment with different physical structures and tasks, it is very close to reality to assume that they are independent. Thus, according to (19), the standard uncertainty of a measurement chain can be obtained from the two related normal distributions using the moment-generating function of those normal distributions. The moment-generating function for a typical normal distribution with the mean $\mu$ and the variance $\sigma^2$ is defined as $e^{\mu.t+\frac{\sigma^2.t^2}{2}}$. According to the statistical theorems, if two independent random variables are combined, the moment-generating function for the new random variable is obtained from the product of moment-generating functions of the independent variables [36].

$$\varphi_{chain}(t) = \varphi_{IT}(t).\varphi_{PMU}(t) \tag{20}$$

In (20), $\varphi_{IT}(t)$ and $\varphi_{PMU}(t)$ are moment-generating functions for instrument transformers and PMUs, respectively. For all equipment, the probability distribution

**Table 4** Integrated error of measurement chain, including the accuracy classes of protection transducers and PMUs

| Voltage Measurement Chain | | | Current Measurement Chain | | |
|---|---|---|---|---|---|
| Accuracy class | Voltage error (%) | Phase displacement (min) | Accuracy class | Current error at rated primary current (%) | Phase displacement at rated primary current (min) |
| 3P | ±3.67 | ±120.0013 | 5P | ±1.00045 | ±60 |
| 6P | ±6.33 | ±240.00061 | 10P | ±3.00015 | – |

function is a standard normal distribution, meaning that the mean value for all of them is zero ($\mu = 0$). Therefore, the moment-generating function of a measurement chain can be expressed as:

$$\varphi_{chain}(t) = e^{0.5\sigma_{IT}^2.t^2}.e^{0.5\sigma_{PMU}^2.t^2} \tag{21}$$

or

$$\varphi_{chain}(t) = e^{0.5(\sigma_{IT}^2+\sigma_{PMU}^2)t^2} \tag{22}$$

It concludes that the distribution of combination of two normally distributed independent variables is another normal distribution which has mean $\mu_{chain}$ and standard deviation $\sigma_{chain}$ as:

$$\begin{aligned} \mu_{chain} &= \mu_{IT} + \mu_{PMU} = 0 \\ \sigma_{chain} &= \sqrt{\sigma_{IT}^2 + \sigma_{PMU}^2} \end{aligned} \tag{23}$$

Therefore, using (10) to (23), the error of a measurement chain can be calculated directly via (24) and the related weight coefficients can be obtained through (15) to (18).

$$e_{Total}^F = \sqrt{\left(e_{IT}^F\right)^2 + \left(e_{PMU}^F\right)^2} \tag{24}$$

The maximum errors of the measurement chains given in Table 4 have been calculated by (24) based on the maximum allowable errors of voltage and current given in Table 2. In most of the studies in the literature, just the PMU errors have been considered to evaluate the performance of fault location algorithms. However, according to Table 4, the main part of measurement error is related to the IT error, i.e. the integer part of the combined error is related to the IT errors, while its decimal part is due to the PMU errors. As shown in Table 4, IT errors are much higher than PMU errors and it is unreasonable to ignore them.

The new approach proposed in this section can be used for calculating the maximum combinational error of each measurement chain.

## 4 Modified Three-Phase State Estimation Formulation for Fault Location

In this section a new method for recognition of fault occurrence, discrimination of the faulty line, estimation of fault location and identification of fault type is proposed based on three-phase state estimation for all fault types including three-phase faults, line-to-line faults, double line-to-ground faults, and single-line-to-ground faults.

Installed PMUs provide the magnitude and phase angle values of the measured quantities to the algorithm. To explain the proposed algorithms, Fig, 4 is presented. Figure 4a shows transmission line $ij$ when a fault $f$ occurs at distance $d_f$ from bus $i$. Figure 4b shows three-phase details of Fig. 4a for a single-line-to-ground fault including phase $c$.

### *4.1 Fault Location as a Hypothetical Bus*

In the proposed algorithm, the fault point (point $f$) on the faulty line (line $ij$) is considered as a hypothetical bus during the fault. As a result, the original $N_{bus}$-bus system can be considered as a $N_{bus} + 1$-bus system and the fault current is recognized as the injected current to the hypothetical bus.

Since there is no measurement equipment on the hypothetical bus, in the modified state estimation problem seven new state variables including the magnitude and phase angle of three-phase voltages of the hypothetical bus along with the fault position are added to the original state variables vector. Therefore, in the modeling of the

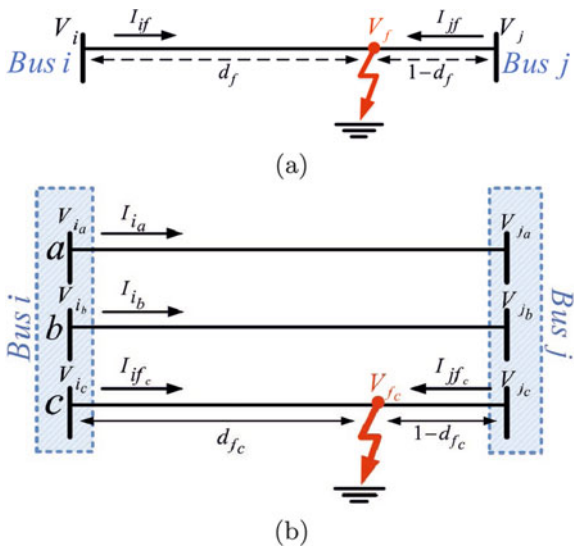


**Fig. 4** Transmission line $ij$ during a fault occurred at distance $d_f$ from the $i$-th bus **a** Single line diagram **b** Single-line-to-ground fault on phase $c$

fault location problem based on the state estimation procedure, the vector of the state variables, $\overline{x}_{modified}$ is expressed as:

$$\overline{x}_{modified} = \left[ \overline{x}^{T}{}_{original} \mid \underbrace{\overline{\theta}^{V}{}_{f_{ph}}^{T} \; \overline{V}_{f_{ph}}^{T} \; d_f}_{\overline{x}_{added}} \right]_{6N_{bus}+7} \tag{25}$$

where $\overline{\theta}^{V}{}_{f_{ph}}$, $\overline{V}_{f_{ph}}$, and $d_f$ are the phase angle and magnitude vectors of three-phase voltages at the hypothetical bus $f$ and the fault location, respectively. It is observed that the number of state variables added to the modified problem is constant for all fault types. In this case, the Jacobian matrix is modified as (26).

$$H_{modified} = \left[ H_{original} \;\middle|\; \frac{\partial \overline{h}(\overline{x}_{modified})}{\partial \overline{x}_{added}} \right] \tag{26}$$

where $H$ is the Jacobian matrix of original $N_{bus}$-bus system and $H_{modified}$ is the modified Jacobian matrix corresponding to $\overline{x}_{modified}$ for the fault location purpose. As the number of network measurements before and during the fault are constant, the number of rows of matrix $H_{modified}$ does not change with respect to $H$, and the number of columns which are added to matrix $H$ are equal to the number of variables added to the state variables.

## 4.2 Bad Data Detection

One of the advantages of state estimation formulation is the systematic capability for dealing with measurement errors. The inherent errors of the measurement chain are modeled by the covariance matrix of errors. On the other hand, due to reasons such as components failure, being under vibration or inappropriate installation environment, some measurement equipment might encounter errors much higher than those listed in Table 4. This kind of resulted data is called bad data. In this study, the largest residual vector is used to identify bad data. For this purpose, after solving the modified state estimation problem, the measurement residual vector is calculated using (27):

$$r(\widehat{\overline{x}}) = \overline{z} - \overline{h}(\widehat{\overline{x}}) \tag{27}$$

where $\widehat{\overline{x}}$ indicates the final value of state variable vector. In order to determine the normalized residual vector, the residual of the covariance matrix must first be calculated as:

$$\Omega(\widehat{\overline{x}}) = R - H(\widehat{\overline{x}}).G^{-1}(\widehat{\overline{x}}).H^{t}(\widehat{\overline{x}}) \tag{28}$$

Then, the elements of the normalized measurement residual vector are calculated as:

$$r_{i_{ph}}^{N}(\widehat{x}) = \frac{r_{i_{ph}}(\widehat{x})}{\sqrt{\Omega_{ii_{ph}}(\widehat{x})}} \tag{29}$$

where, $\Omega_{ii_{ph}}$ indicates the elements of residual covariance diagonal matrix ($\Omega$) corresponding to the $i$-th measurement and $r_{i_{ph}}$ is the $i$-th element of the measurement residual vector. After calculating the normalized measurement residual vector, its largest element is determined and selected.

If the value of the largest element of the normalized residual vector ($r_{\max}^{N}$) is greater than the pre-determined threshold ($\left|r_i^N\right| > \beta$), this means that the measurement corresponding to this element contains bad data. For bad data detection by the largest residual vector, the distinctive threshold $\beta$ is usually selected equal to 3 in the literature such as [36, 37]. The choice of $\beta = 3$ as the threshold in references is based on the experiences related to huge tests and stochastic theories. In addition we have tested the threshold $\beta$ equal to 3 by too much fault scenarios on different test system for the measurement chains errors more than those given in Table 4. For all studied scenarios, the elements corresponding to the failed measurement in the measurement residual normalized vector have been greater than 3. When the bad data is detected, the two following actions can be performed to improve the state estimation results; correcting bad data using estimated values of the state variables or solving the modified state estimation problem again by removing the faulty measurement from the measurement values vector, in case of data redundancy.

### *4.3 Observability and Data Redundancy*

The magnitude and phase angle of three-phase voltages at $N_{bus}$ buses, magnitude and phase angle of the hypothetical bus at fault point and the distance of fault point from one end of the faulty line for three phases should be determined by WLS algorithm. Thus, the number of the variables in the proposed fault location formulation is $6N_{bus} + 7$. In the fault location problem based on the state estimation technique, similar to a conventional state estimation problem, the best solution is obtained when the problem is in the over-determined condition. The over-determined condition refers to the condition in which the number of the measurements ($3m$) in the network is greater than the number of the variables ($n = 6N_{bus} + 7$). However, in order to take advantage of detecting and removing bad data, the number of measurements must be more than the variables ($3m \gg 6N_{bus} + 7$). Thus the redundancy of measurements determined the number of bad data which can be detected. The redundancy technique can be realized by more measurements or using two or several data sets related to different time instants during the fault period.

## *4.4 Proposed Algorithm*

The proposed fault location algorithm is based on three-phase state estimation which requires three-phase model of the network and transmission lines and three-phase PMU measurements including voltage and current phasors. Thus, the proposed algorithm uses the network data and PMU measurements for detection of faulty line, accurate estimation of fault location and identification of fault type according to the following steps as shown in Fig. 5.

### 4.4.1 Detection of Faulty Line

**Step 1**: If some transmission lines are disconnected from the network, the probable fault incident investigation and possible faulty line discrimination processes are initiated.

**Step 2**: Under normal operation (prior to the line trip), the system situation including the network configuration (breakers status) and system operation quantities are specified by the measurement and monitoring systems. When a fault is occurred on a transmission line, the network configuration becomes different with the initial network configuration. The step 2 of the algorithm considers the initial network configuration along with the last set of data before fault clearing by opening the faulty line circuit breakers for achieving three-phase state estimation.

For more explanation, assume the circuit breakers are opened after 5 cycles from the fault occurrence instant. Thus, if the reporting rate of PMUs be one sample per cycle, then there are 5 set of phasor samples provided by PMUs during the fault. Since there is not compatibility between the system configuration (related to the normal situation) and the measurements used in the state estimation study, the bad data are detected and consequently the current measurements corresponding to the maximum normalized residual vector indicates the faulty line.

Briefly, using the initial network configuration (prior to lines disconnection) and the last set of data before circuit breakers tripping, three-phase state estimation is executed according to (1)–(9). According to (27)–(29) and using the bad data detection process for state estimation results, the normalized residual vector of current measurements would be calculated. The existence of bad data can be due to fault occurrence and the lack of conformity between the network configuration and data used in the executed state estimation. Therefore, there are two possible cases:

1. If bad data is not detected in current measurements, it can be concluded that the fault occurrence is not the cause of circuit breakers tripping.

2. If bad data is detected in current measurements, it means a fault has occurred and the current measurements corresponding to the maximum normalized residual vector indicate the faulty line.

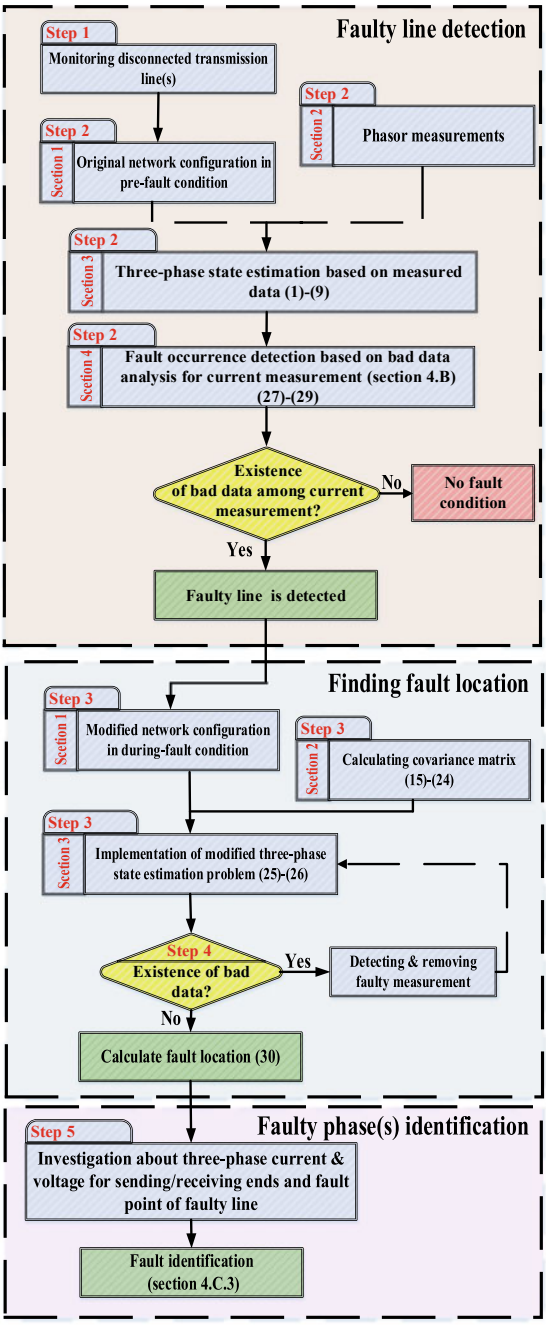


**Fig. 5** Flowchart of proposed method

### 4.4.2 Estimation of Fault Location

**Step 3**: According to (15)–(18) the covariance matrix is calculated based on the maximum possible errors of the measurements given in Table 4. Then the modified three-phase state estimation problem based on (25)–(26) is solved by considering the new state variables added to the state vector.
**Step 4**: Based on the content of Sect. 4.2, bad data analysis is performed to detect the corresponding faulty measurement. If any bad data is detected in the measurements vector, the faulty measurements are removed and the calculation begins again from step 3. This process continues until all faulty measurements are detected and removed. Finally, the fault location is determined with the required accuracy.

### 4.4.3 Identifying Fault Type

**Step 5**: By calculating the modified state vector in (25), the fault location is exactly detected, and also the three-phase voltages of fault point $V_{f_{ph}}$ are calculated. By investigating $V_{f_{ph}}$, $V_{i_{ph}}$, $V_{j_{ph}}$ and currents $I_{if_{ph}}$, $I_{jf_{ph}}$ (Fig. 4) during the fault, the fault type and the phase or phases contributing to the fault can be identified according to the power system short circuit theory.

## 5 Simulation Results

The performance of the proposed method has been investigated using several IEEE test systems. Since the transmission network of these systems are inherently symmetrical network, to demonstrate the benefit of the proposed method, the symmetric networks are converted to asymmetric networks in the following steps according to [36].

1. Based on $Z_1$ (positive sequence impedance) of the lines given by the data set of networks, $Z_2$ (negative sequence impedance) and $Z_0$ (zero sequence impedance) of the network lines are set as:

$$\begin{aligned} Z_2 &= Z_1 \\ Z_0 &= 3Z_1 \end{aligned} \tag{30}$$

2. The sequence impedance matrix ($Z_{012}$) for each transmission line is formed as:

$$Z_{012} = \begin{bmatrix} Z_0 & 0 & 0 \\ 0 & Z_1 & 0 \\ 0 & 0 & Z_2 \end{bmatrix} \tag{31}$$

3. The phase impedance matrix ($Z_{abc}$) for each transmission line is calculated as:

$$Z_{abc} = \begin{bmatrix} Z_{aa} & Z_{ab} & Z_{ac} \\ Z_{ba} & Z_{bb} & Z_{bc} \\ Z_{ca} & Z_{cb} & Z_{cc} \end{bmatrix} = T^{-1}.Z_{012}.T \tag{32}$$

where

$$T = \begin{bmatrix} 1 & 1 & 1 \\ 1 & e^{j120} & e^{j240} \\ 1 & e^{j240} & e^{j120} \end{bmatrix} \tag{33}$$

In the $Z_{abc}$ calculated by (32), the mutual impedance between phases, $Z_{ab}$, $Z_{bc}$, and $Z_{ac}$ are equal. To model non-perfect transposition of the lines phases according to [36]:

$$\begin{aligned} Z_{ab} &= Z_{bc} \\ Z_{ac} &= 0.6 Z_{ab} \end{aligned} \tag{34}$$

The $Z_{abc}$ of lines calculated as above presents asymmetric lines and are used in the three-phase state estimation. The fault location algorithm need to knowing the network topology and parameters. About 1 million fault studies on different test systems (IEEE 9, 14, 39, 57 and 118-bus test networks) have been demonstrated excellent performance of the proposed method. In this section, some results related to the modified IEEE 118-bus test system [42, 43] are only presented. The fault simulation was performed using the PowerFactory environment [41] and the related data were processed using appropriate softwares. The simulations were performed on a PC with an Intel Core i7 CPU including 32GB of RAM. Usually, the PMUs are located to attain observability of network under normal operation. For example, to realize complete observability conditions, studies of [44] have been led to locate 28 PMUs on buses 3, 8, 11, 12, 17, 21, 25, 28, 34, 35, 40, 45, 49, 53, 56, 62, 72, 75, 77, 80, 85, 86, 90, 94, 102, 105, 110 and 114 of 118-bus system as shown in Fig. 6. However, these PMUs cannot guarantee the observability during faults, thus, it is required to complete the initial set with other PMUs for attaining fault observability and encountering bad data, inherent error of measurement chains and parameter errors. These purpose are achieved by adding three PMUs at buses 47, 61 and 63 in the 118-bus system. However, this choice is not unique and the accurate results in fault location and detection of some measurement and parameter errors can be alternatively obtained by adding three PMUs to buses 51, 64 and 70. It is evident that the incorrect choices of PMUs cannot guarantee the results for the proposed algorithm. For example, adding PMUs at buses 57, 74 and 84 in addition to 28 initial PMUs leads to unacceptable errors in fault location for some cases such as faults occurred on line 64-65. In addition, the studies have been demonstrated that adding only one or two PMUs cannot provide full fault observability in presence of measurement errors. We have specified the required PMUs with heuristic methods; however, the optimal locations can be specified by the systematic methods such as ones in [45]. Consequently, the optimal number and locations of PMUs are determined based on

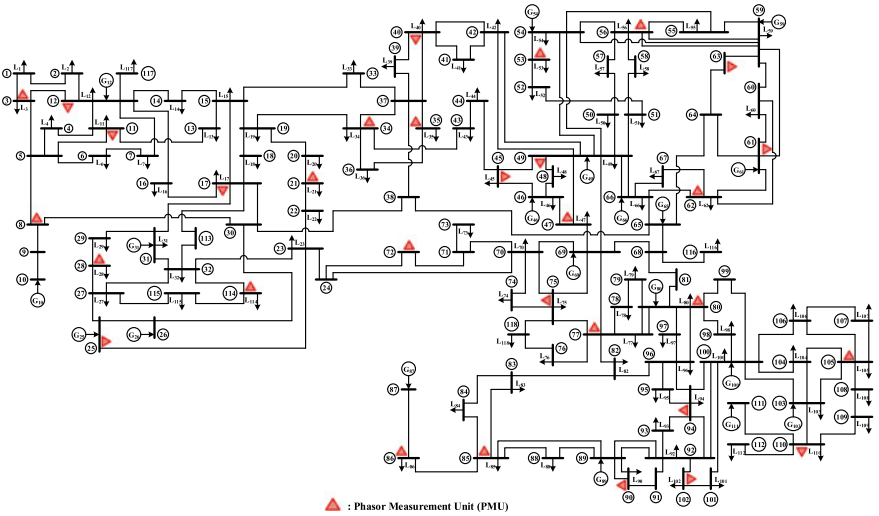


**Fig. 6** IEEE 118-bus system

defining an appropriate optimization problem with required rules related to the state observability and fault observability.

In simulations, measurement chain errors have randomly been generated using the normal distribution based on the maximum allowable value given in Table 4. The simulated errors very closely reflect real measuring conditions. Numerous fault events have been simulated on different locations of all network transmission lines of the test systems. For each fault, 100 cases of added random errors to the measurement vector were considered. Then, for each location scenario, the relative error of fault location algorithm is calculated as the average of 100 simulated cases according to (35).

$$FLE(\%) = \frac{1}{100}\sum_{s=1}^{100}\frac{\left|d_{f,s}^{est} - d_f^{true}\right|}{d_{Line}} \times 100\% \tag{35}$$

where $FLE$ is the relative error of the algorithm's result for each location scenario, $d_{f,s}^{est}$ is the estimated location of fault for the $s$-th case, $d_f^{true}$ is the actual location of the fault, and $d_{Line}$ is the length of the line.

## *5.1 Faulty Line Discrimination*

The performance of the proposed method for discrimination of the faulty line was investigated by simulation of different fault scenarios on all 177 lines of the IEEE 118-bus system. It is observed that the method correctly performs for all the tested

**Table 5** Results for a fault on line (3-5)

| | | | | | | | |
|---|---|---|---|---|---|---|---|
| Faulty line discrimination | Bad data results for current measurements | | | | | | |
| | Bad data solution | $r^N_{\max}$ | Corresponding measurement | | measured in bus | | |
| | 1st | 18.742 | $I_{3-5}$ | | 3 | | |
| | 2nd | 16.449 | $I_{5-3}$ | | 5 | | |
| | Faulty line | Line (3-5) | | | | | |
| Fault identification | Estimated faulty line quantities (p.u.) | | | | | | |
| | Quantities | Voltage magnitude | | | Current magnitude | | |
| | Phase | $a$ | $b$ | $c$ | $a$ | $b$ | $c$ |
| Bus | Sending | 0.951 | 0.198 | 0.981 0.381 | 9.523 | 0.275 | |
| | Hypothetical | 0.941 | 0.000 | 0.993 | – | – | |
| | Receiving | 0.848 | 0.191 | 0.971 | 0.396 | 6.317 | 0.302 |
| | Fault data | True | | | Estimated | | |
| | $d_f$ (p.u.) | 0.2 | | | 0.20041 | | |
| | Type | SLG | | | SLG | | |
| | Faulty phase | $b$ | | | $b$ | | |
| | $FLE$ (%) | 0.041% | | | | | |

scenarios. For example, consider a single-phase-to-ground short-circuit including phase $b$ occurred on line connected between buses 3 and 5 at 20% distance from bus 3. At first, the measured phasors related to during fault (before opening of circuit breakers of two sides of the line) and the basic network configuration in the three-phase state estimation problem are used to solve the problem. In this case, the maximum normalized residual is obtained as 18.742 which corresponds to the measured current $I_{3-5}$. The second maximum normalized residual vector is 16.449 which corresponds to the measured current $I_{5-3}$. These results indicate that line (3–5) can be a faulty line candidate. Then, the bad data are eliminated by solving the modified three-phase estimation problem with the hypothetical bus on line (3–5). The results of solving the problem for line 5 are shown in Table 5. These results demonstrate very high accuracy of the fault location and fault type identification.

### 5.2 Importance of Matrix R and Measurement Chain Error Modeling in the Fault Location Algorithm

In Sect. 3, we discussed about the calculation method of the maximum error of measurement chains using the maximum allowable errors of PMUs and transducer transformers. The maximum error of measurement chains is used to correctly construct the measurement errors covariance matrix, $R$, which is required in the state estimation formulation. In this section, the importance of correct construction of matrix $R$ and also modeling the measurement chains error is studied. For this purpose, random measurement errors are generated using the measurement chain error model proposed in Sect. 3. Then matrix $R$ is constructed considering two different assumptions as follow.

$Case1$ : The error of instrument transformers are not considered in the measurement chains error and matrix $R$ is only constructed based on PMUs errors.

$Case2$ : Matrix $R$ is accurately constructed based on the measurement chains errors.

Table 6 gives the average of $FLE$s obtained from the proposed fault location algorithm for two cases 1 and 2 applied on numerous different fault scenarios on the transmission lines of IEEE 118-bus test system. It is observed that the errors of fault location algorithm are not acceptable in case 1. The large $FLE$s in this case are due to the mismatch between the real measurement error and incorrect assumption in the construction of matrix $R$. The obtained outcomes confirm significance of accurate measurement chain modeling in obtaining truthful results which is properly performed in this chapter.

### 5.3 Study of Bad Data Detection in the Measurement Vector

One of the important aspects of the proposed method is detecting bad data. A comprehensive study of bad data detection has been performed by adding various biased errors to different PMU measurements. The proposed method correctly identifies the failed measurements for all cases. Here the results of a few studied cases are presented. These cases are related to the occurrence of all fault types on line (16-17) with added biased error to measurement chain of bus 11 as:

$Case1$ : Adding simultaneous errors to magnitude and phase angle of voltage phasor of bus 11. The errors of magnitude and phase angle are set as 20% and 10 degrees, respectively.

$Case2$ : Adding simultaneous errors to either magnitude or phase angle of current phasors of lines (11-12) at bus 11 and (11–13) at bus 11. The errors of magnitude and phase angle are considered as 20% and 10 degrees, respectively.

Table 7 summarizes the results of these case studies. For each case, the two left columns provide the maximum of the normalized residual vector corresponding to the failed measurements. After removing the failed measurements from the data set

**Table 6** Impact of matrix $R$ and measurement chains error modeling in the fault location algorithm

| Line No./ $FLE$ (%) | Case 1 | Case 2 | Line No./$FLE$ (%) | Case 1 | Case 2 | Line No./ $FLE$ (%) | Case 1 | Case 2 | Line No. /$FLE$ (%) | Case 1 | Case 2 | Line No./ $FLE$ (%) | Case 1 | Case 2 | Line No./ $FLE$ (%) | Case 1 | Case 2 |
|---|---|---|---|---|---|---|---|---|---|---|---|---|---|---|---|---|---|
| Line 1–2 | 3.614 | 0.257 | Line 19–34 | 3.312 | 0.169 | Line 40–41 | 2.918 | 0.089 | Line 55–59 | 2.289 | 0.11 | Line 76–77 | 3.646 | 0.173 | Line 92–94 | 3.703 | 0.118 |
| Line 1–3 | 4.679 | 0.161 | Line 20–21 | 2.418 | 0.334 | Line 40–42 | 2.177 | 0.114 | Line 56–57 | 3.094 | 0.149 | Line 77–78 | 3.587 | 0.073 | Line 93–94 | 3.067 | 0.17 |
| Line 2–12 | 2.705 | 0.31 | Line 21–22 | 4.234 | 0.223 | Line 41–42 | 4.76 | 0.308 | Line 56-58 | 4.506 | 0.271 | Line 77–80 C1 | 2.855 | 0.126 | Line 94–100 | 3.602 | 0.153 |
| Line 3–12 | 3.432 | 0.263 | Line 22–23 | 3.14 | 0.055 | Line 42–49 C1 | 2.865 | 0.19 | Line 56–59 C1 | 2.565 | 0.043 | Line 77–80 C2 | 2.06 | 0.251 | Line 94–95 | 3.335 | 0.125 |
| Line 3-5 | 4.567 | 0.272 | Line 23–24 | 4.564 | 0.197 | Line 42–49 C2 | 2.455 | 0.065 | Line 56–59 C2 | 4.404 | 0.225 | Line 77–82 | 2.036 | 0.307 | Line 94–96 | 3.841 | 0.201 |
| Line 4–11 | 3.845 | 0.316 | Line 23–25 | 2.945 | 0.094 | Line 43–44 | 3.894 | 0.271 | Line 59–60 | 2.712 | 0.2 | Line 78–79 | 4.419 | 0.014 | Line 95–96 | 4.001 | 0.163 |
| Line 4–5 | 4.196 | 0.086 | Line 23–32 | 2.097 | 0.241 | Line 44-45 | 4.449 | 0.249 | Line 59–61 | 2.568 | 0.222 | Line 79-80 | 3.84 | 0.215 | Line 96–97 | 2.601 | 0.135 |
| Line 5-11 | 2.828 | 0.14 | Line 24–70 | 2.433 | 0.078 | Line 45–46 | 2.573 | 0.097 | Line 60–61 | 4.183 | 0.15 | Line 80–96 | 4.414 | 0.102 | Line 98–100 | 3.255 | 0.276 |
| Line 5–6 | 3.036 | 0.318 | Line 24–72 | 4.703 | 0.147 | Line 45-49 | 3.401 | 0.104 | Line 60–62 | 4.473 | 0.218 | Line 80-97 | 3.179 | 0.114 | Line 99–100 | 2.757 | 0.286 |
| Line 6–7 | 3.304 | 0.312 | Line 25–27 | 2.747 | 0.062 | Line 46-47 | 3.256 | 0.074 | Line 61–62 | 3.845 | 0.263 | Line 80-98 | 4.567 | 0.27 | Line 100–101 | 4.503 | 0.25 |
| Line 7–12 | 3.717 | 0.105 | Line 26–30 | 4.245 | 0.16 | Line 46–48 | 4.073 | 0.055 | Line 62–66 | 3.269 | 0.017 | Line 80–99 | 2.18 | 0.098 | Line 100–103 | 4.841 | 0.102 |

(continued)

**Table 6** (continued)

| Line No./ $FLE$ (%) | Case 1 | Case 2 | Line No./$FLE$ (%) | Case 1 | Case 2 | Line No./ $FLE$ (%) | Case 1 | Case 2 | Line No. /$FLE$ (%) | Case 1 | Case 2 | Line No./ $FLE$ (%) | Case 1 | Case 2 | Line No./ $FLE$ (%) | Case 1 | Case 2 |
|---|---|---|---|---|---|---|---|---|---|---|---|---|---|---|---|---|---|
| Line 8–9 | 4.022 | 0.273 | Line 27–115 | 4.465 | 0.315 | Line 47–49 | 3.733 | 0.334 | Line 62–67 | 2.982 | 0.269 | Line 82–83 | 2.514 | 0.251 | Line 100–104 | 3.138 | 0.127 |
| Line 8–30 | 4.055 | 0.013 | Line 27–28 | 2.768 | 0.266 | Line 47–69 | 4.238 | 0.282 | Line 63–64 | 2.581 | 0.147 | Line 82–96 | 2.215 | 0.189 | Line 100–106 | 4.022 | 0.133 |
| Line 9–10 | 2.617 | 0.159 | Line 27–32 | 4.307 | 0.081 | Line 48–49 | 2.081 | 0.199 | Line 64–65 | 3.908 | 0.28 | Line 83–84 | 2.146 | 0.153 | Line 101–102 | 3.517 | 0.076 |
| Line 11–12 | 2.904 | 0.155 | Line 28–29 | 4.161 | 0.324 | Line 49–50 | 3.048 | 0.274 | Line 65–68 | 2.314 | 0.288 | Line 83–85 | 2.282 | 0.234 | Line 103–104 | 2.724 | 0.158 |
| Line 11–13 | 2.467 | 0.146 | Line 29–31 | 4.191 | 0.23 | Line 49–51 | 3.259 | 0.313 | Line 66–67 | 2.853 | 0.196 | Line 84–85 | 2.102 | 0.272 | Line 103–105 | 3.527 | 0.259 |
| Line 12–117 | 4.411 | 0.115 | Line 30–38 | 3.701 | 0.207 | Line 49–54 C1 | 2.22 | 0.203 | Line 68–116 | 2.987 | 0.218 | Line 85–86 | 2.384 | 0.202 | Line 103–110 | 4.368 | 0.209 |
| Line 12–14 | 4.347 | 0.055 | Line 31–32 | 2.319 | 0.082 | Line 49–54 C2 | 3.689 | 0.023 | Line 68–81 | 4.778 | 0.1 | Line 85–88 | 3.464 | 0.281 | Line 104–105 | 2.967 | 0.304 |
| Line 12–16 | 3.337 | 0.126 | Line 32–113 | 3.159 | 0.3 | Line 49-66 C1 | 3.961 | 0.2 | Line 69–70 | 2.979 | 0.176 | Line 85-89 | 2.662 | 0.104 | Line 105–106 | 4.181 | 0.058 |
| Line 13–15 | 3.892 | 0.334 | Line 32-114 | 3.024 | 0.202 | Line 49–66 C2 | 3.094 | 0.167 | Line 69–75 | 2.633 | 0.324 | Line 86–87 | 3.271 | 0.306 | Line 105–107 | 4.324 | 0.037 |
| Line 14–15 | 3.092 | 0.229 | Line 33–37 | 4.133 | 0.287 | Line 49–69 | 3.701 | 0.077 | Line 69–77 | 2.344 | 0.25 | Line 88–89 | 2.63 | 0.161 | Line 105–108 | 3.077 | 0.269 |

(continued)

**Table 6** (continued)

| Line No./ $FLE$ (%) | Case 1 | Case 2 | Line No./$FLE$ (%) | Case 1 | Case 2 | Line No./ $FLE$ (%) | Case 1 | Case 2 | Line No. /$FLE$ (%) | Case 1 | Case 2 | Line No./ $FLE$ (%) | Case 1 | Case 2 | Line No./ $FLE$ (%) | Case 1 | Case 2 |
|---|---|---|---|---|---|---|---|---|---|---|---|---|---|---|---|---|---|
| Line 15–17 | 3.622 | 0.1 | Line 34–36 | 4.326 | 0.114 | Line 50–57 | 3.642 | 0.242 | Line 70–71 | 2.847 | 0.246 | Line 89–90 C1 | 3.995 | 0.257 | Line 106–107 | 4.144 | 0.193 |
| Line 15–19 | 2.365 | 0.032 | Line 34–37 | 3.861 | 0.328 | Line 51–52 | 3.011 | 0.133 | Line 70–74 | 4.347 | 0.312 | Line 89–90 C2 | 4.633 | 0.173 | Line 108–109 | 2.036 | 0.338 |
| Line 15–33 | 3.062 | 0.023 | Line 34–43 | 4.304 | 0.217 | Line 51–58 | 3.182 | 0.056 | Line 70–75 | 2.646 | 0.122 | Line 89-92 C1 | 2.578 | 0.1 | Line 109-110 | 4.146 | 0.268 |
| Line 16–17 | 2.776 | 0.14 | Line 35–36 | 3.637 | 0.047 | Line 52–53 | 3.702 | 0.06 | Line 71–72 | 3.85 | 0.136 | Line 89–92 C2 | 2.866 | 0.135 | Line 110–111 | 3.571 | 0.193 |
| Line 17–113 | 4.204 | 0.095 | Line 35–37 | 2.612 | 0.14 | Line 53–54 | 2.517 | 0.236 | Line 71–73 | 3.362 | 0.057 | Line 90–91 | 2.666 | 0.058 | Line 110–112 | 3.7 | 0.111 |
| Line 17–18 | 4.682 | 0.218 | Line 37–39 | 4.354 | 0.317 | Line 54-55 | 2.888 | 0.244 | Line 74–75 | 4.254 | 0.296 | Line 91-92 | 4.747 | 0.279 | Line 114–115 | 4.39 | 0.193 |
| Line 17–31 | 2.963 | 0.208 | Line 37–40 | 3.38 | 0.013 | Line 54–56 | 4.735 | 0.07 | Line 75–118 | 3.714 | 0.301 | Line 92–100 | 3.695 | 0.185 | | | |
| Line 18–19 | 4.737 | 0.104 | Line 38–65 | 2.655 | 0.166 | Line 54–59 | 2.695 | 0.293 | Line 75–77 | 4.569 | 0.319 | Line 92–102 | 3.916 | 0.289 | | | |
| Line 19-20 | 2.257 | 0.074 | Line 39–40 | 2.075 | 0.244 | Line 55–56 | 2.949 | 0.316 | Line 76–118 | 3.991 | 0.157 | Line 92–93 | 4.821 | 0.123 | | | |

**Table 7** Results of bad data detection in the measurement vector

| Fault Type | Case 1 | | | | Case 2 | | | |
|---|---|---|---|---|---|---|---|---|
| | 1st iteration FLE(%) | Failed magnitude measurement $r^N_{\max}$ | Failed phase angle measurement $r^N_{\max}$ | Last iteration FLE(%) | 1st iteration FLE(%) | Failed magnitude measurement $r^N_{\max}$ | Failed phase angle measurement $r^N_{\max}$ | Last iteration FLE(%) |
| A-G | 9.854 | 18.971 | 17.93 | 0.286 | 12.688 | 23.272 | 21.342 | 0.388 |
| B-G | 10.692 | 21.459 | 18.173 | 0.198 | 11.782 | 23.585 | 19.697 | 0.253 |
| C-G | 8.715 | 19.391 | 17.242 | 0.268 | 12.145 | 23.848 | 19.491 | 0.306 |
| AB | 8.392 | 19.23 | 16.839 | 0.267 | 12.172 | 21.878 | 17.223 | 0.217 |
| AC | 9.717 | 20.023 | 18.231 | 0.093 | 12.468 | 21.005 | 18.961 | 0.174 |
| BC | 9.633 | 19.806 | 18.108 | 0.044 | 13.436 | 24.092 | 18.59 | 0.224 |
| AB-G | 9.148 | 20.212 | 18.143 | 0.125 | 11.195 | 20.998 | 18.712 | 0.382 |
| AC-G | 9.355 | 18.36 | 17.008 | 0.165 | 14.542 | 24.087 | 20.387 | 0.222 |
| BC-G | 9.053 | 19.924 | 18.894 | 0.223 | 12.131 | 20.182 | 17.543 | 0.272 |
| ABC | 9.692 | 20.934 | 16.139 | 0.232 | 14.139 | 21.855 | 18.506 | 0.215 |
| ABC-G | 8.857 | 20.434 | 18.171 | 0.13 | 13.17 | 20.374 | 18.889 | 0.365 |

and solving the modified state estimation using the sound data, the average $FLE$ of fault location algorithm is given in the right column for each case.

For example, considering an A-G fault in the first case, when the solving process is performed, the $r^N_{\max}$, which corresponds to the magnitude of voltage measurement of bus 10, is obtained as 24.536, which is significantly higher than the distinctive threshold ($\beta = 3$). Then, after removing this faulty measurement, the solution process is repeated. The value of $r^N_{\max}$ in the second repetition is also greater than $\beta = 3$ and equals to 21.044 which corresponds to the phase error of voltage measurement of bus 10. In the third repetition, the value of $r^N_{\max}$ reaches to less than 3 and $FLE$ becomes equal to 0.024%. The calculated $FLE$ is much less than 1%, which is usually considered as an acceptable error for the fault location algorithms.

As shown, in all simulated cases, the failed measurements were detected correctly and after removing the faulty measurement from the solving process, the fault location was estimated with an acceptable accuracy. In all cases, the $FLE$s are less than 0.37%.

## *5.4 Impact of Different Data Redundancy Methods on the Proposed Algorithm*

As a necessary condition, there should be always redundancy in the measurements vector to obtain the best estimation for the fault location in the presence of measure-

**Table 8** Comparison of $FLE(\%)$ for different methods of providing data redundancy

| | Fault type | A-G | B-G | C-G | AB | AC | BC | AB-G | AC-G | BC-G | ABC | ABC-G |
|---|---|---|---|---|---|---|---|---|---|---|---|---|
| Methods | | | | | | | | | | | | |
| Method A | | 0.011 | 0.017 | 0.084 | 0.086 | 0.097 | 0.084 | 0.081 | 0.042 | 0.017 | 0.087 | 0.041 |
| Method B | | 0.025 | 0.264 | 0.099 | 0.289 | 0.308 | 0.136 | 0.127 | 0.308 | 0.297 | 0.143 | 0.197 |

ment chain inherent errors and bad data. One of the ways to create data redundancy is access to more voltage and current phasors. An alternative way is using multiple samples of measured quantities during the fault interval with the same number of measurements.

In the first method (method A), we assume that the measurements of voltage phasors and current phasors in the network of IEEE 118-bus test system are available according to the aforementioned 31 PMUs as shown in Fig. 6, while in the second method (method B), there are only 28 PMUs located at buses 3, 8, 11, 12, 17, 21, 25, 28, 34, 35, 40, 45, 49, 53, 56, 62, 72, 75, 77, 80, 85, 86, 90, 94, 102, 105, 110 and 114 according to [44]. In both methods, the number of measurements is more than the minimum requirement for full observability of the system. In method A, one phasor sample of each measurement is used but in the second method, two phasors related to the time interval before circuit breaker opening are used as inputs to the algorithm.

According to Table 8, the obtained results for various types of faults in the 118-bus system show that in both methods, data redundancy has enabled the algorithm to detect fault location with a high degree of accuracy. Furthermore, it can be realized that in the proposed algorithm, only the existence of measurement data redundancy is sufficient for detecting and eliminating faulty measurements, but how to generate data redundancy has no major effect on the algorithm process and the accuracy of the fault location algorithm.

## *5.5 A Discussion on the Speed of the Proposed Algorithm*

The fault location algorithms are developed to accurate estimation of the fault point on transmission lines to identify the weak network points in the case of the temporary faults or reduce the repair time in the case of the permanent faults. Thus, in contrast to protective algorithms, the speed of the fault location algorithm and related algorithms such as the algorithm of identifying the faulted line is not a main and important aspect. In fact, these algorithms are offline ones and executed after the protection system operation. However, Table 9 compares the speed and accuracy of the proposed algorithm with a number of the existing PMU-based fault location algorithms. The average execution time of the proposed algorithm and six existing PMU-based fault location algorithms for different fault scenarios on IEEE 118-bus system [33, 46–

**Table 9** Average execution time of proposed algorithm in comparison with six existing PMU-based fault location algorithms for different fault scenarios on IEEE 118-bus system

| Methods | Proposed method | [52] | [46] | [47] | [48] | [49] | [50] |
|---|---|---|---|---|---|---|---|
| Execution time | 0.088 * | 0.49 | 0.079 | 7.7 | 0.61 | 1.09 | 0.328 |
| Average $FLE$ (%) | 0.23 | 0.47 | 0.65 | 0.61 | 0.31 | 0.51 | 0.84 |

* The execution time is calculated for average execution time of scenarios with three bad measurements detection and fault location calculation

**Table 10** Minimum, maximum and average execution time of proposed algorithm on different test networks

| Test network | Proposed method | | |
|---|---|---|---|
| | Min. execution time* | Max. execution time** | Average execution time |
| IEEE 14 bus | 0.028 s | 0.056 s | 0.044 s |
| IEEE 39 bus | 0.051 s | 0.081 s | 0.073 s |
| IEEE 57 bus | 0.061 s | 0.088 s | 0.079 s |
| IEEE 118 bus | 0.078 s | 0.97 s | 0.089 s |

* The execution time is calculated for average execution time of scenarios with two bad measurements detection and fault location calculation

** The execution time is calculated for average execution time of scenarios with five bad measurements detection and fault location calculation

50] gives in Table 9 demonstrate the execution time of the most methods such as the proposed method is fraction of 1 Sec. The minimum, average and maximum times of the proposed algorithm execution for four test systems with different sizes are given in Table 10, also demonstrates the execution time increases with the system size although the times are still small.

Table 10 demonstrates the execution time increases with the system size although the times are still small. The presented methods in this chapter can be modified for different applications in power systems operation, control, protection and security [33, 51, 53–56].

## 6 Conclusions

In this chapter, a fault location algorithm for transmission lines based on the three-phase state estimation formulation is proposed. The proposed modified formulation integrates all tasks including fault occurrence recognition, faulty line discrimination, fault location estimation and fault type and faulty phase(s) identification. It exploits the excellent capacities of three-phase state estimation for analyzing all symmetrical and asymmetrical faults on transposed and untransposed lines, reducing the

effect of inherent errors of measurements chain on the fault location accuracy and detecting and eliminating the bad data in the measurement vector. The algorithm's performance has been investigated by simulating numerous fault cases on different locations of the transmission lines of the modified 39-bus test system with an asymmetric network. For each of the fault cases, the inherent errors of the measurements chain are considered in the measurement vector based on the proposed error model of the measurements chain. It was demonstrated that for all cases, the error of fault location algorithm is much less than 0.5%. In addition, the importance of correct construction of measurement error covariance matrix as one of the effective parameters on the state estimation calculation has been investigated. The proposed error model of the measurement chain uses the maximum allowable errors of PMUs and transducer transformers to calculate the maximum errors of the measurement chains utilized to correctly construct matrix $R$.

## References


1. AIEE Committee Report,:Bibliography and summary of fault location methods [includes discussion]., Trans. American Institute of Electrical Engineers. Part III: Power Apparatus and Systems, vol. 74, no. 3, pp. 1423– 1428. (1955)
2. R.J. Hamidi, H. Livani, Traveling-wave-based fault-location algorithm for hybrid multiterminal circuits. IEEE Trans. Power Del. **32**(1), 135–144 (2017)
3. IEEE Std. C37.114-2014 (Rev. IEEE Std. C37.114-2004),: IEEE guide for determining fault location on ac transmission and distribution lines, pp. 1–76, (2015)
4. F. Deng, X. Zeng, X. Tang, Z. Li, Y. Zu, L. Mei, Travelling-wave-based fault location algorithm for hybrid transmission lines using three-dimensional absolute grey incidence degree. International Journal of Electrical Power & Energy Systems **114**, 105306 (2020)
5. Akmaz, D., Salih Mami, M., Arkan, M., Emin Taluk, M.,: Transmission line fault location using traveling wave frequencies and extreme learning machine, Electric Power Systems Research, vol. 155, pp. 1–7, (2018)
6. O. Naidu, A.K. Pradhan, A Traveling Wave-Based Fault Location Method Using Unsynchronized Current Measurements. IEEE Transactions on Power Delivery **34**, 505–513 (2019)
7. E.J.S. Leite, F.V. Lopes, F.B. Costa, W.L.A. Neves, Closed-Form Solution for Traveling Wave-Based Fault Location on Non-Homogeneous Lines. IEEE Transactions on Power Delivery **34**, 1138–1150 (2019)
8. O.A. Gashteroodkhani, M. Majidi, M. Etezadi-Amoli, A.F. Nematollahi, B. Vahidi, A hybrid SVM-TT transform-based method for fault location in hybrid transmission lines with underground cables. Electric Power Systems Research **170**, 205–2014 (2019)
9. C. Fei, G. Qi, C. Li, Fault location on high voltage transmission line by applying support vector regression with fault signal amplitudes. Electric Power Systems Research **160**, 173–179 (2018)
10. Y.Q. Chen, O. Fink, G. Sansavini, Combined Fault Location and Classification for Power Transmission Lines Fault Diagnosis With Integrated Feature Extraction. IEEE Transactions on Industrial Electronics **65**, 561–569 (2018)
11. J. Izykowski, R. Molag, E. Rosolowski, M.M. Saha, Accurate location of faults on power transmission lines with use of two-end unsynchronized measurements. IEEE Trans. Power Del. **21**(2), 627–633 (2006)
12. Ahmed, A. S., Attia, M. A., Hamed, N. M., Abdelaziz, A. Y.,: Modern optimization algorithms for fault location estimation in power systems, international journal of Engineering science and technology, vol. 20, no. 5, pp. 1475–1485, (2017)

13. D. Akmaz, M.S. Mamiş, M. Arkan, M.E. Tğluk, Transmission line fault location using traveling wave frequencies and extreme learning machine. Elec. Power Sys. Research **155**, 1–7 (2018)
14. Dalcastagne, A. L., Zimath, S. L.,: A study about the sources of error of impedance-based fault location methods. In: Transmission and distribution conference and exposition, pp. 1–6, IEEE/PES, Latin America (2008)
15. R.A. de Aguiar, A. Dalcastagnê, H.H. Zürn, R. Seara, Impedance-based fault location methods: Sensitivity analysis and performance improvement. Elec. Power Sys. Research **155**, 236–245 (2018)
16. Dalcastagnê, A., Noceti Filho, S., Zurn, H., Seara, R.,: An iterative two-terminal fault-location method based on unsynchronized phasors, IEEE Trans. Power Del., vol. 23, no. 4, pp. 2318–2329, (2008)
17. Y. Liao, N. Kang, Fault-location algorithms without utilizing line parameters based on the distributed parameter line model. IEEE Trans. Power Del. **24**(2), 579–584 (2009)
18. J. Izykowski, E. Rosolowski, P. Balcerek, M. Fulczyk, M.M. Saha, Accurate noniterative fault-location algorithm utilizing two-end unsynchronized measurements. IEEE Trans. Power Del. **26**(2), 547–555 (2011)
19. J. Doria-Garcia, C. Orozco-Henao, L.U. Iurinic, J.D. Pulgarn-Rivera, High impedance fault location: Generalized extension for ground faults. International Journal of Electrical Power & Energy Systems **114**, 105387 (2020)
20. Didehvar, S., Mohammadi Chabanloo, R.,: Accurate estimating remote end equivalent impedance for adaptive one-ended fault location, Electric Power Systems Research, vol. 170, pp. 194–204, (2019)
21. T. Spielbck, A. Bel, Design of a one-sided, impedance-based transmission line fault locator using line topology and source impedances. Electric Power Systems Research **161**, 123–128 (2018)
22. M.A. Elsadd, A.Y. Abdelaziz, Unsynchronized fault-location technique for two- and three-terminal transmission lines. Electric Power Systems Research **158**, 228–239 (2018)
23. M. Ghazizadeh-Ahsaee, Accurate arcing fault location method for M-terminal transmission lines. International Journal of Electrical Power & Energy Systems **98**, 147–155 (2018)
24. Y. Lee, T. Lin, C. Liu, Multi-Terminal Non-homogeneous Transmission Line Fault Location Utilizing Synchronized Data. IEEE Transactions on Power Delivery **34**, 1030–1038 (2019)
25. A.G. Phadke, J.S. Thorp, K.J. Karimi, State estimation with phasor measurements. IEEE Trans. Power Sys. **1**(1), 233–238 (1986)
26. S. Azizi, M. Sanaye-Pasand, A straightforward method for wide-area fault location on transmission networks. IEEE Trans. Power Del. **30**(1), 264–272 (2015)
27. Saha, M. M., Izykowski, J., Rosolowski, E.,: Fault location on power networks, Springer Science & Business Media, (2009)
28. Q. Jiang, B. Wang, X. Li, An efficient PMU-based fault-location technique for multi terminal transmission lines. IEEE Trans. Power Del. **29**(4), 1675–1682 (2014)
29. D. Sayari, P.S. Shiv, K.P. Bijaya, Transmission line fault detection and location using Wide Area Measurements. Elec. Power Sys. Research **151**, 96–105 (2017)
30. A.H. Al-Mohammed, M.A. Abido, An adaptive fault location algorithm for power system networks based on synchrophasor measurements. Elec. Power Sys. Research **108**, 153–163 (2014)
31. S. Azizi, M. Sanaye-Pasand, M. Paolone, Locating faults on untransposed, meshed transmission networks using a limited number of synchrophasor measurements. IEEE Trans. Power Sys. **31**(6), 4462–4472 (2016)
32. Mahamedi, B., Sanaye-Pasand, M., Azizi, S., Zhu, J. G.,: Unsynchronised fault-location technique for three-terminal lines, IET Gen., Trans. & Distrib., vol. 9, no. 15, pp. 2099–2107, (2015)
33. M. Majidi, M. Etezadi-Amoli, M.S. Fadali, A sparse-data-driven approach for fault location in transmission networks. IEEE Trans. Smart Grid **8**(2), 548–556 (2017)
34. M.A. Elsadd, A.Y. Abdelaziz, Unsynchronized fault-location technique for two- and three-terminal transmission lines. Elec. Power Sys. Research **158**, 228–239 (2018)

35. S. Hussain, A.H. Osman, Fault location on series and shunt compensated lines using unsynchronized measurements. Elec. Power Sys. Research **116**, 166–173 (2014)
36. A. Ghaedi, M.E.H. Golshan, M. Sanaye-Pasand, Transmission line fault location based on three-phase state estimation framework considering measurement chain error model. Electric Power Systems Research **178**, 106048 (2020)
37. A. Gomez-Exposito, A. Abur, *Power system state estimation: theory and implementation* (CRC Press, 2004)
38. IEEE Std. C57.13-2016 (Revision of IEEE Std C57.13-2008): IEEE standard requirements for instrument transformers, pp. 1–96, (2016)
39. Alstom,: Network protection & automation guide. Alstom grid, (2011)
40. IEEE Std. C37.118.1-2011 (Revision of IEEE Std. C37.118-2005),: IEEE standard for synchrophasor measurements for power systems, pp. 1–61, (2011)
41. DIgSILENT GmbH, PowerFactory v15.2.6 software, https://www.digsilent.de/en/powerfactory.html
42. Information Trust Institute Grainger College of Engineering, IEEE 118-Bus System, https://icseg.iti.illinois.edu/ieee-118-bus-system
43. University of Washington, Power Systems Test Case Archive, http://labs.ece.uw.edu/pstca/pf118/pg_tca118bus.htm
44. F. Aminifar, A. Khodaei, M. Fotuhi-Firuzabad, M. Shahidehpour, Contingency-constrained PMU placement in power networks. IEEE Trans. Power Sys. **25**(1), 516–523 (2010)
45. M.E.H. Golshan, S.H.H. Dolatabadi, S.M. Tabatabaei, Determining minimum number and optimal placement of PMUs for fault observability in one-terminal algorithms. IET Generation, Transmission & Distribution **12**(121), 5789–5797 (2018)
46. G. Feng, A. Abur, Identification of faults using sparse optimization, *52nd Annual Allerton Conference on Communication*, Control, and Computing (Allerton) (IEEE, Allerton, 2014), pp. 1040–1045
47. Q. Jiang, X. Li, B. Wang, H. Wang, PMU-based fault location using voltage measurements in large transmission networks. IEEE Trans. on power Del. **27**(3), 1644–1652 (2012)
48. A.S. Dobakhshari, Fast accurate fault location on transmission system utilizing wide-area unsynchronized measurements. International Journal of Electrical Power & Energy Systems **101**, 234–242 (2018)
49. S. Das, S.P. Singh, B.K. Panigrahi, Transmission line fault detection and location using wide area measurements. Electric Power Systems Research **151**, 96–105 (2017)
50. C. Wang, C.X. Dou, X.B. Li, Q.Q. Jia, A WAMS/PMU-based fault location technique. Electric Power Systems Research **77**(8), 936–945 (2007)
51. H.H. Alhelou, M.H. Golshan, J. Askari-Marnani, Robust sensor fault detection and isolation scheme for interconnected smart power systems in presence of RER and EVs using unknown input observer. International Journal of Electrical Power & Energy Systems **99**, 682–694 (2018)
52. H.H. Alhelou, M.E. Hamedani-Golshan, R. Zamani, E. Heydarian-Forushani, P. Siano, Challenges and opportunities of load frequency control in conventional, modern and future smart power systems: A comprehensive review. Energies **11**(10), 2497 (2018)
53. Haes Alhelou, H., Hamedani Golshan, M. E., Hajiakbari Fini, M.,: Wind driven optimization algorithm application to load frequency control in interconnected power systems considering GRC and GDB nonlinearities, Electric Power Components and Systems, 46(11-12), 1223-1238, (2018)
54. Haes Alhelou, H., Hamedani-Golshan, M. E., Njenda, T. C., Siano, P.,: A survey on power system blackout and cascading events: Research motivations and challenges, Energies, 12(4), 682, (2019)
55. H.H. Alhelou, M.E.H. Golshan, N.D. Hatziargyriou, A decentralized functional observer based optimal LFC considering unknown inputs, uncertainties, and cyber-attacks. IEEE Transactions on Power Systems **34**(6), 4408–4417 (2019)
56. H.H. Alhelou, M.E.H. Golshan, N.D. Hatziargyriou, Deterministic dynamic state estimation-based optimal lfc for interconnected power systems using unknown input observer. IEEE Transactions on Smart Grid (2019)